International Journal of Precision Engineering and Manufacturing-Green Technology (2021) 8:47–55
https://doi.org/10.1007/s40684-019-00163-9
Online ISSN 2198-0810
Print ISSN 2288-6206

REGULAR PAPER

Realization of Superhydrophobic Surfaces Based on Three-Dimensional Printing Technology

Beomchan Kang[1] · Jaebum Sung[1] · Hongyun So[1,2]

Received: 9 April 2019 / Revised: 27 September 2019 / Accepted: 1 October 2019 / Published online: 25 October 2019

Abstract

A superhydrophobic surface was successfully realized using fused deposition modeling-type three-dimensional (3D) printing technology. The low printing resolution (400 µm) and various printing angles from 0° to 90° were employed to print the mold for casting of polymer surfaces. The polymer surface cast from the mold exhibited waveform microstructures that had a tilting angle almost identical to the printing angle. The maximum average water contact angle (WCA) of fabricated polymer surfaces was 160°, which is much higher than that of flat (bare) polymer surfaces (up to 52.3% increase in the WCA). In particular, water droplets immediately rolled off along 8°-tilted surfaces, cast from the mold printed with printing angle of 70°. This demonstrated the superhydrophobic property. The result of this study shows the feasibility of a facile, rapid, inexpensive, and effective microfabrication of superhydrophobic surfaces using the current 3D printing technology.

Keywords 3D printing · Printing angle · Superhydrophobic surface · Waveform microstructure · Rapid microfabrication

1 Introduction

The control of the water contact angle (WCA), or wettability, of solid surfaces is a core technique in a wide variety of applications in fields ranging from the micro- to the macro-scale [1–4]. For example, the fluid dynamics of two-phase flows and the mixing of two laminar flows in microchannels highly depend on the wettability [5–8], and a high WCA can prevent (or delay) frost formation on surfaces, thus extending the lifetime of mechanical/electrical systems in cold environments [9–12]. Based on the magnitude of the WCA, the physical property of an arbitrary surface can be classified into four groups, namely superhydrophilicity, hydrophilicity, hydrophobicity, and superhydrophobicity [13]. In particular, studies regarding superhydrophobic surfaces have emerged in various fields including mechanical, electrical, chemical, and biomedical engineering, because the superhydrophobicity has multiple functions such as filtration [14–16], delay of frost formation [11, 17], self-cleaning [18–20], and fluidic drag reduction [21–23]. In general, a solid surface is considered as a superhydrophobic surface when the surface has a static WCA more than 150° and a rolling-off angle less than 10° [13, 24]. To fabricate superhydrophobic surfaces, various methods including laser ablation [25, 26], plasma etching [27, 28], chemical etching [29], coating [30, 31], and sol–gel processes [32, 33] have been widely investigated. However, most of methods require complicated procedures and chemical treatments, which can limit an extensive adoption of superhydrophobic surfaces to large-scale applications. The fabrication of superhydrophobic polymer surface with hierarchical structures has been developed recently using hot imprinting process, but it required a thermal treatment process at a high temperature [34]. In addition to superhydrophobicity, icephobicity is another essential surface property that can easily be controlled by surface treatments [35, 36]. Ice formation on solid surfaces can cause significant damage to various systems such as degradation of thermal transfer efficiency in heat exchangers [37, 38] and decrease in sensitivity of optical instruments [39]. Although superhydrophobic surfaces are not always icephobic because of different mechanisms of water and ice adhesion [40–43], the key technique for creating an icephobic surface is to lower the ice adhesion strength of the surface by providing sufficient voids at the interface, which is closely related to the superhydrophobicity [35]. Consequently, a facile, rapid,

✉ Hongyun So
hyso@hanyang.ac.kr

[1] Department of Mechanical Engineering, Hanyang University, Seoul 04763, South Korea

[2] Institute of Nano Science and Technology, Hanyang University, Seoul 04763, South Korea

and high-throughput fabrication of superhydrophobic surfaces is highly demanded to overcome drawbacks of conventional manufacturing methods.

In the past decade, three-dimensional (3D) printing technology has emerged as a facile, cost-effective, and rapid prototyping method for various manufacturing applications [44–47]. Among a variety of printing methods, the fused deposition modeling (FDM) technique is the most common and user-friendly method, because 3D structures can be easily designed using computer-aided design (CAD) and directly printed by stacking fused filaments [48–50]. However, a critical disadvantage of the FDM-based printing method is rough surfaces of the end products, which are typically caused by low printing resolution and filaments piled up in layers [51, 52]. To reduce the degree of roughness, a higher printing resolution is required, which increases the printing time and cost for manufacturing. In our previous study, we demonstrated that this drawback (i.e., rough surface) of 3D-printed molds can be used to fabricate 3D hydrophobic polymer surfaces [53]. In this study, we demonstrated that this drawback of 3D-printed structures can be further effectively used for the microfabrication of superhydrophobic surfaces, and investigated the effect of printing angles on wettability of surfaces. In other words, superhydrophobic surfaces could be realized from the 3D-printed mold by controlling the printing angle as a parameter. When the casting mold was printed with the resolution of 400 µm and printing angle of 70°, the surface cast from the mold exhibited superhydrophobic properties (i.e., WCA of ~ 154.7° and a water droplet sliding angle of 8°). This study supports that the superhydrophobic surfaces can be easily and quickly fabricated using an additive manufacturing (3D printing) technology compared to complicated and multiple procedures in conventional microfabrication methods.

2 Experimental Section

2.1 Materials

To prepare a casting mold for creating superhydrophobic surfaces, flat molds with different printing angles were first designed using a computer-aided design (CAD) software (NX11, Siemens) and printed using a FDM-type 3D printer (GUIDER II, FlashForge, China). The printing conditions of printing speed, extruder temperature, and platform temperature were set to 80 mm/s, 220 °C, and 50 °C, respectively. The printing density was experimentally determined as 15%, which can minimize printing time, but still print sufficient details for the mold. A polylactic acid (PLA) filament with a diameter of 1.75 mm, which is a commonly used filament for FDM printing methods [54, 55], was employed in this study. Figure 1 shows the schematic of the overall fabrication process for creating a superhydrophobic polymer surface from 3D-printed mold. As a first step, a casting mold was printed with different printing angles from 0° to 90°. The main mold part was printed with the support part, which

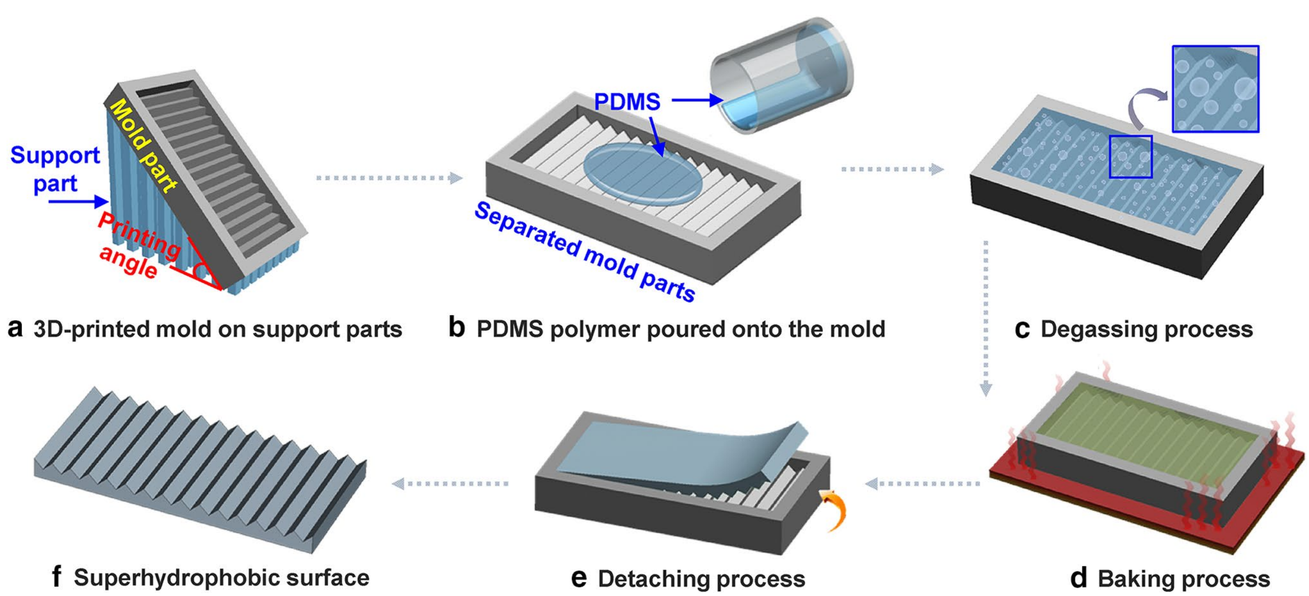

Fig. 1 Schematic of overall fabrication process for superhydrophobic polymer surfaces using 3D-printed mold: **a** printing a mold with a support parts using different printing angles, **b** pouring PDMS prepolymer onto the mold detached from the support part, **c** degassing process to remove air bubbles, **d** baking process to cure prepolymer, **e** detaching cured PDMS from the mold, and **f** finalizing superhydrophobic surfaces

provides the tilted printing angle, as shown in Fig. 1a. The molds inclined at 60°, 70°, and 80° could be printed without the support part because the threshold overhang angle [56] was set at approximately 33.6° from the vertical in the 3D printer used in this study. However, the support part was intentionally applied to all molds for a consistent printing condition. Although a shape of support structures can also affect the surface roughness of the mold [57, 58], it affects only the bottom of the mold where the support part is directly in touch with the mold. Based on the printing angle, the stacking direction of PLA filament can be intentionally controlled, thus generating different shapes of microstructures on the final products. After detaching the main mold part from the support part (by simply separating them by hand), the PDMS mixture (prepolymer: curing agent = 10: 1) was poured onto the main mold (Fig. 1b). To remove air bubbles that were generated during the pouring process, the degassing process was performed in a vacuum chamber at room temperature (Fig. 1c). The PDMS mixture was then baked at 45 °C for 7 h for the polymerization process (Fig. 1d), and a detaching process was followed from the 3D-printed main mold (Fig. 1e). The cured PDMS polymer was easily and cleanly detached from the PLA mold without any chemical treatment between the PDMS and PLA mold surface (Fig. 1f). The 3D-printed mold can also be used repeatedly to generate the same PDMS polymer surface, supporting the rapid, cost-effective, and high-throughput manufacturing method to create a superhydrophobic surface. Finally, the detached PDMS polymer surface was characterized experimentally to demonstrate superhydrophobic properties.

2.2 Testing and Characterization

2.2.1 Water Contact Angle Analysis

Superhydrophobic properties of the fabricated PDMS polymer surfaces were experimentally characterized using values of the WCA measured by a water contact angle goniometer (Phoenix-MT(A), Surface Electro Optics, Korea). To compare the WCA on various PDMS surfaces cast from PLA molds printed with different printing angles, a static WCA was measured by image-processing software (Image Pro 300). At least five measurements of WCA were performed, and the average value of WCA was determined. To investigate the effect of the printing angle on the WCA value, the cross-sectional shape of the fabricated PDMS polymer surface was analyzed using an optical camera (ViTiny UM12, MicroLinks Technology Corp.). The pitch distance and peak-to-valley height between microstructures were then measured.

2.2.2 Water Droplet Roll-Off Test

To characterize the wettability and adhesive properties of the fabricated PDMS surfaces, a water roll-off test was carried out using a syringe and video recording software (Camtasia 9, TechSmith Corp.). The fabricated PDMS surface was placed on 8°- and 10°-tilted substrates, and water droplets were repeatedly dropped onto random positions of the fabricated PDMS surface to demonstrate superhydrophobic properties. This procedure was repeated at least eight times to obtain reliable data for wettability analysis.

3 Results and Discussion

Figure 2a shows the schematic of the main mold parts on support parts designed by CAD software with respect to varied printing angles from 0° to 90°. It should be noted that the different printing angle creates different staircase-shaped microstructures on the mold surface owing to the varied stacking direction of PLA filament. The printing angle eventually affects the wettability and WCA values of the PDMS surface cast from the main mold. Figure 2b shows the actual image of mold products printed using a 3D printer. In this study, the printing resolution of 400 μm and all printing angles (i.e., from 0° to 90°) were tested to print main molds for superhydrophobic surfaces. In our previous work, because the WCA on the polymer surface cast from the PLA mold tended to have higher WCA as the printing resolution decreased [53], the lowest printing resolution (400 μm) was employed to create superhydrophobic surfaces in this study. The printing running durations for printing of the main mold (dimensions: 54 mm × 29 mm × 6 mm) were 0.21, 0.33, 0.45, 0.48, 0.51, 0.53, 0.4, 0.41, 0.33, and 0.21 h for the printing angles of 0°, 10°, 20°, 30°, 40°, 50°, 60°, 70°, 80°, and 90°, respectively. This rapid printing running time can realize the rapid prototyping and manufacturing method for the reusable platform of superhydrophobic surfaces.

To investigate the surface morphology of PDMS polymers cast from the 3D-printed PLA molds, the fabricated bulk polymer was cut by a razor blade, and the cross-sectional image was captured using an optical microscope, as shown in Fig. 3a. An array of waveform (or waveshape) microstructures were uniformly generated by casting from the 3D-printed molds. The valley area (i.e., area between individual microstructure) represents the region where the PLA filament existed. It should also be noted that the direction of waveform microstructures varied depending on the printing angle (see Figs. 3a and 4 for detail). For example, tips of waveform microstructures cast from the PLA mold printed with 40° had a tilt to the one (left) side, while those cast from the PLA mold printed with 90° were generated in the direction perpendicular to the substrate, as shown in Fig. 4.

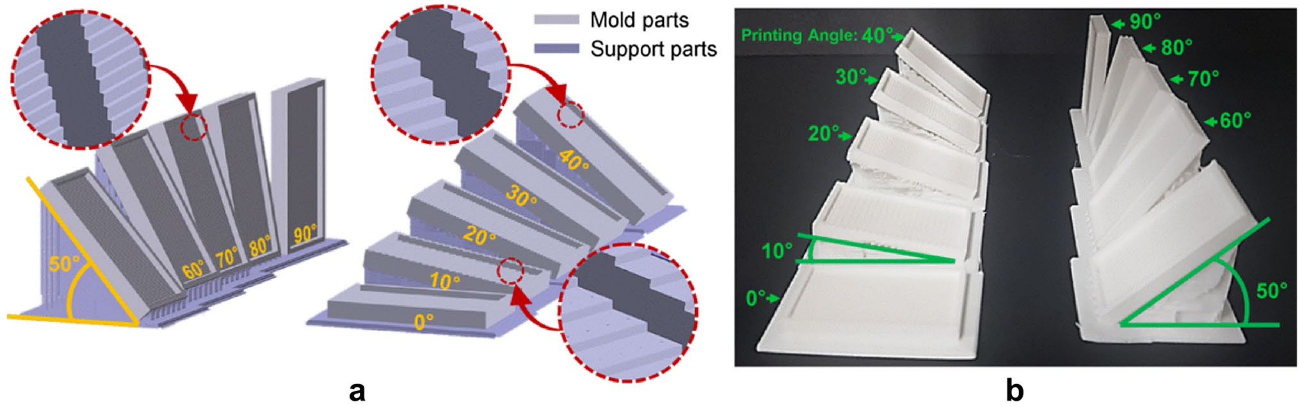

Fig. 2 **a** CAD images of main 3D mold parts on support parts with respect to various printing angles and **b** actual image of mold products printed by a 3D printer. Different printing angles create different staircase-shaped microstructures on the mold surface owing to the varied stacking direction of PLA filament. Each staircase-shaped microstructure generated by different printing angles has different roughness as shown in zoomed-in view in **a**

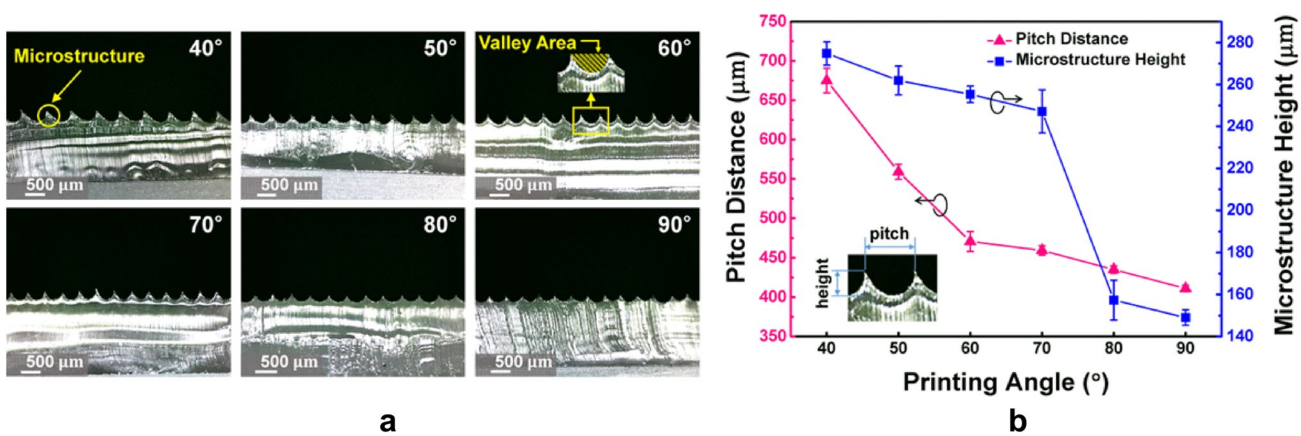

Fig. 3 **a** Optical image of PDMS polymer surface cast from 3D-printed PLA mold (cross-sectional view) and **b** pitch distance between microstructures and height of microstructure as a function of the printing angle from 40° to 90°

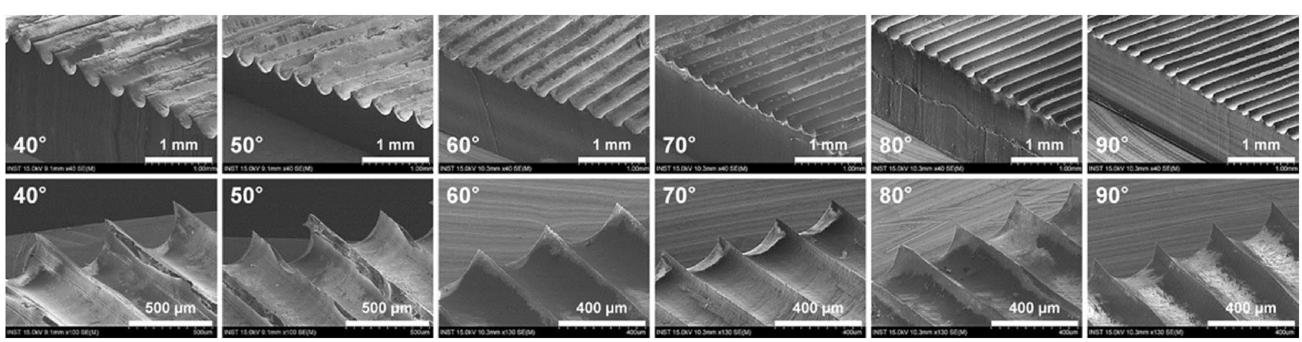

Fig. 4 SEM images of waveform microstructures cast from 3D-printed PLA mold (first row: zoomed-out and second row: zoomed-in view). Based on the printing angle, the tilted direction of waveform microstructures can be controlled owing to obliquely stacked PLA filaments

This is primarily because PLA filaments were obliquely stacked along with the printing angle (see Fig. 1a), thus creating the different tilted angles of waveform microstructures. Figure 3b shows the pitch distance and height of the individual waveform microstructure depending on the printing angle. As the printing angle increased, both pitch distance and height of microstructure decreased because of obliquely stacked PLA filaments, which depend on the printing angle. Figure 5a shows the correlation between the tilted angle of waveform microstructures and the printing angle of PLA molds. The tilted angle of each surface was experimentally measured using the image editing software and cross-sectional optical image of PDMS polymer surfaces, as shown in Fig. 5b. As the printing angle increased, the tilted angle of microstructure increased linearly. It should also be noted that values of the tilted angle are very close to those of printing angle. That means the tilted angle of microstructure on surfaces can be easily modified without complicated manufacturing processes. In other words, the pitch distance, height, and tilted angle of waveform microstructures can be easily controlled by simply changing the printing angle.

To characterize the effect of the printing angle on WCA, a water droplet was dropped onto each surface through a syringe and the WCA value was measured using a water contact angle goniometer. Figure 6 shows the measured WCA on each PDMS polymer surfaces cast from the 3D-printed PLA molds depending on the printing angle. It should be noted that the measured WCA values on surfaces with the printing angles larger than 40° exceeded 150°, which meets one of conditions for superhydrophobic surfaces. Compared to the WCA of approximately 105° on the flat PDMS surface, the PDMS surface cast from the PLA mold printed with the printing angle of 90° formed an average WCA of 160° (~52.3% increase in WCA), as shown in Fig. 6. As the printing angle of the PLA mold increased, the value of WCA increased simultaneously. This might be because as the tilted angle of the waveform microstructures increased from 0° to 90° (i.e., as the printing angle of the PLA mold increased), the surface contact area between the water (liquid) and waveform microstructures (solid) continuously reduced, thus resulting in higher WCA (nearly spherical water droplet) [59]. Consequently, the surfaces with a high WCA were easily and quickly achieved using a 3D-printed mold compared to expensive etching processes and complicated chemical treatments in conventional methods, as listed in Table 1.

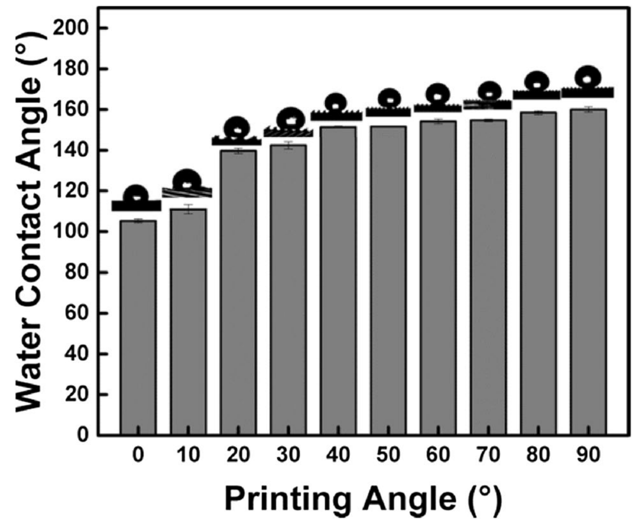

Fig. 6 WCA values on each PDMS polymer surfaces cast from the 3D-printed PLA molds depending on the printing angle. It should be noted that WCA on surfaces with the printing angles larger than 40° exceed 150°. Inset: optical image of the water droplet on each surface

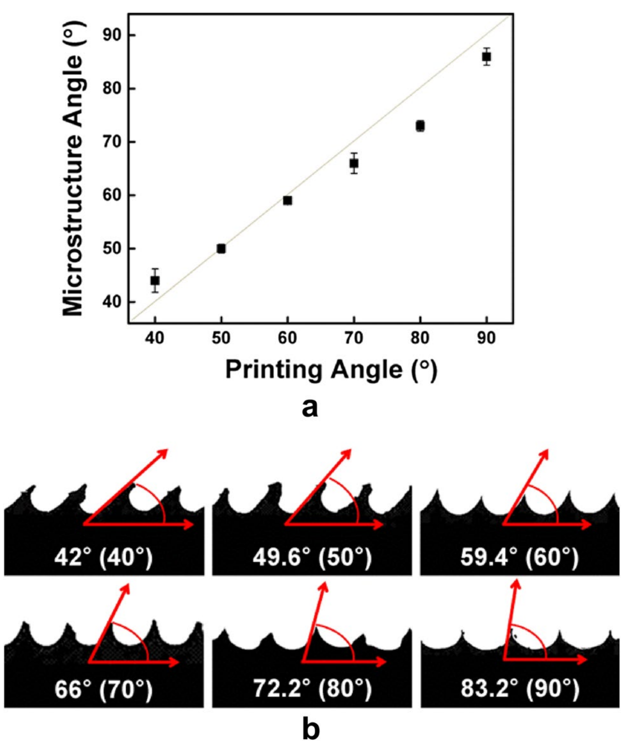

Fig. 5 **a** Correlation between microstructure angle (i.e., tilted angle of waveform microstructures) of PDMS polymer surfaces and printing angle of PLA main molds. **b** Optically measured values of tilted angle of waveform microstructures with respect to printing angle (values in parentheses). It should be noted that the microstructure angle is approximately matched with the printing angle

Table 1 Comparison of fabrication methods and maximum WCA

Material	Method	Max. WCA	References
PDMS	Laser ablation	154.5°	[25]
PDMS	Laser ablation	171°	[26]
Wood	Plasma etching + chemical coating	161.2	[27]
PDMS	Plasma etching + chemical coating	169°	[28]
Aluminum	Chemical etching + coating	163.7°	[29]
Glass	Sol–gel	169°	[32]
PDMS	Cast from 3D-printed mold	160°	This work

To demonstrate the superhydrophobic property, a roll-off test on each PDMS polymer surface was performed to characterize the wettability. Figure 7a, b show the sequential images of the water droplet rolled off on the 10°-tilted PDMS polymer surface cast from the PLA mold printed with the printing angle of 60° (WCA of ~ 154.2°) and 70° (WCA of ~ 154.7°), respectively. The direction of the waveform microstructure tips was set to the left side. The water droplets on both polymer surfaces immediately rolled off when the titling angle of surface reached 10°. However, water droplets on PDMS polymer surfaces cast from the mold printed with 40°, 50°, 80°, and 90° were not continuously rolled off along the surface. This might be because surfaces cast from molds printed at a printing angle of 60° and 70° showed the highest aspect ratio value (a ratio of the height of microstructures to the pitch distance), as shown in Fig. 8. This high aspect ratio provides the most sufficient air gaps at the liquid/solid interface and helps water droplets slide readily [60]. To further investigate the most superhydrophobic surface, the roll-off test was performed on 8°-tilted surface. As a result, the water droplets rolled off on the polymer surface cast from the PLA mold printed at a printing angle of 70° only, as shown in Fig. 7c. This implied that the optimal tilted angle of waveform microstructure for the superhydrophobic surface was 70°. In conclusion, the facile and rapid fabrication of the superhydrophobic polymer surface (i.e., WCA of ~ 154.7° and sliding at tilted angle of 8°) was realized using the 3D printing technology without the use of complicated micromachining and chemical surface treatments. To further develop the method for achieving

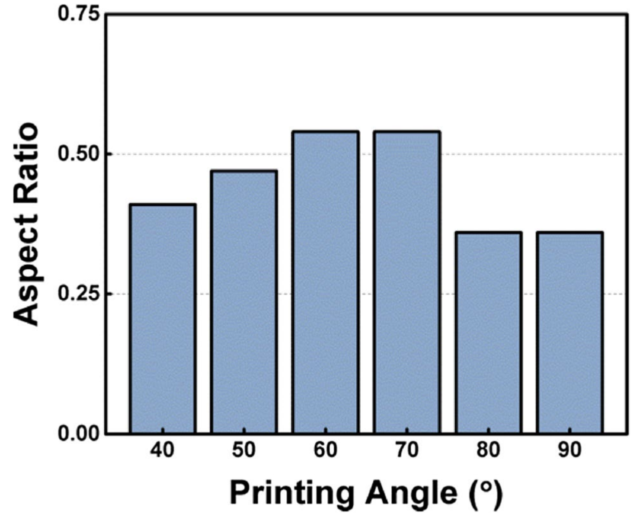

Fig. 8 Aspect ratio (= structure height/pitch distance) of microstructures as a function of printing angle from 40° to 90°

superhydrophobic surfaces from hydrophilic materials, further studies will be required to optimize the angle and shape of microstructures.

4 Conclusions

In summary, the superhydrophobic surface was successfully realized using a 3D printing technology. To cast the PDMS polymer surface from the 3D-printed mold, an FDM-type

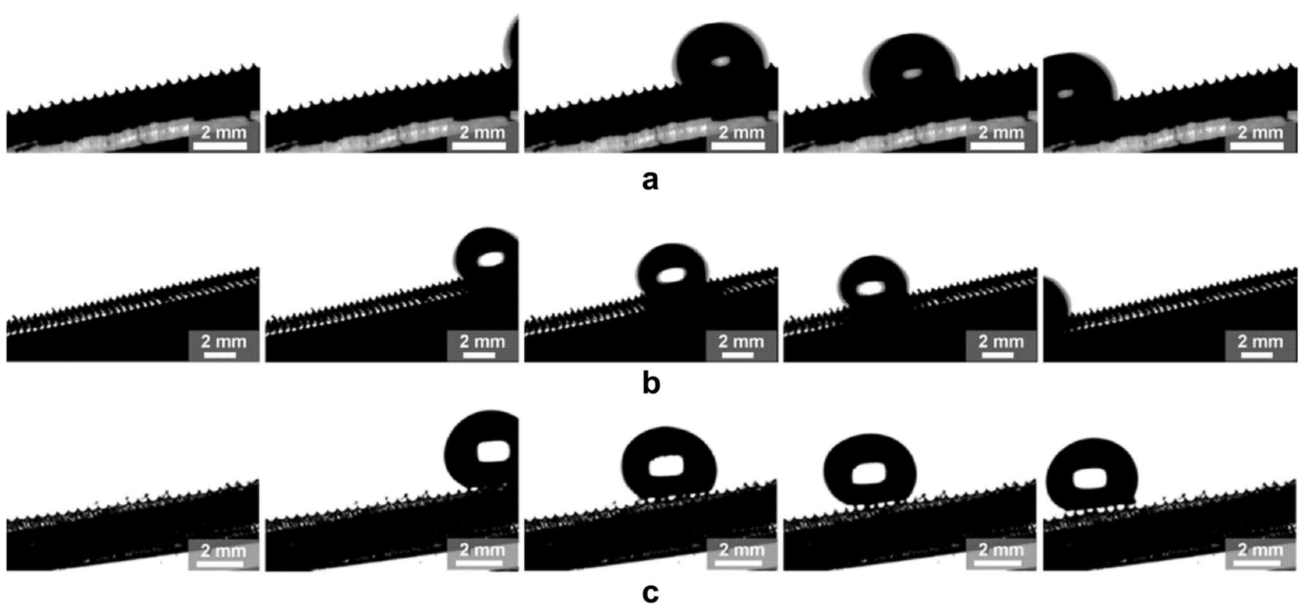

Fig. 7 Sequential images of a water droplet rolled off on the 10°-tilted PDMS polymer surface cast from PLA mold printed with printing angle of **a** 60° and **b** 70°. **c** Roll-off test on the 8°-tilted PDMS polymer surface cast from PLA mold printed with printing angle of 70°

3D printer was employed with PLA filaments as the printing material. The PDMS polymer surface cast from the 3D-printed PLA mold showed an array of waveform microstructures, and the tilted angle of those structures varied by the printing angle. The value of tilted angle of waveform microstructures was almost identical to the printing angle, indicating that the tilted angle of microstructures on the surface can be easily controlled by the setting of the 3D printer. The fabricated polymer surfaces showed a maximum 52.3% increase in WCA compared to that on flat PDMS polymer surface. In particular, water droplets were immediately rolled off on 8°-tilted surface cast from the PLA molds printed with the printing angle of 70°, indicating the superhydrophobic surface. This work supports the use of 3D printing technology, which can be employed to rapidly manufacture the superhydrophobic polymer surface without complex micromachining and chemical surface treatment. This demonstrates a facile, cost-effective, rapid, and reliable microfabrication technique for creating the superhydrophobic surface.

Acknowledgements This work was supported by the Human Resources Program in Energy Technology of the Korea Institute of Energy Technology Evaluation and Planning (KETEP), granted financial resource from the Ministry of Trade, Industry & Energy (MOTIE) of the Republic of Korea (no. 20174030201750).

Compliance with Ethical Standards

Conflict of interest There are no conflicts to declare.

References

1. Zhang, X., Shi, F., Niu, J., Jiang, Y., & Wang, Z. (2008). Superhydrophobic surfaces: From structural control to functional application. *Journal of Materials Chemistry, 18,* 621–633.
2. Hong, X., Gao, X., & Jiang, L. (2007). Application of superhydrophobic surface with high adhesive force in no lost transport of superparamagnetic microdroplet. *Journal of the American Chemical Society, 129,* 1478–1479.
3. Peng, C.-W., Chang, K.-C., Weng, C.-J., Lai, M.-C., Hsu, C.-H., Hsu, S.-C., et al. (2013). Nano-casting technique to prepare polyaniline surface with biomimetic superhydrophobic structures for anticorrosion application. *Electrochimica Acta, 95,* 192–199.
4. Liu, F., Ma, M., Zang, D., Gao, Z., & Wang, C. (2014). Fabrication of superhydrophobic/superoleophilic cotton for application in the field of water/oil separation. *Carbohydrate Polymers, 103,* 480–487.
5. Cubaud, T., Ulmanella, U., & Ho, C.-M. (2006). Two-phase flow in microchannels with surface modifications. *Fluid Dynamics Research, 38,* 772–786.
6. Choi, C., Yu, D. I., & Kim, M. (2011). Surface wettability effect on flow pattern and pressure drop in adiabatic two-phase flows in rectangular microchannels with T-junction mixer. *Experimental Thermal and Fluid Science, 35,* 1086–1096.
7. Lim, Y. T., Kim, S.-J., Yang, H., & Kim, K. (2006). Controlling the hydrophilicity of microchannels with bonding adhesives containing surfactants. *Journal of Micromechanics and Microengineering, 16,* N9–N16.
8. Horiuchi, K., Dutta, P., & Richards, C. D. (2007). Experiment and simulation of mixed flows in a trapezoidal microchannel. *Microfluidics and Nanofluidics, 3,* 347–358.
9. He, M., Wang, J., Li, H., Jin, X., Wang, J., Liu, B., et al. (2010). Super-hydrophobic film retards frost formation. *Soft Matter, 6,* 2396.
10. Kim, M.-H., Kim, H., Lee, K.-S., & Kim, D. R. (2017). Frosting characteristics on hydrophobic and superhydrophobic surfaces: A review. *Energy Conversion and Management, 138,* 1–11.
11. So, H., & Park, W. (2019). Attachable freezing-delayed surfaces for ultraviolet sensing using GaN photodetector at low temperature in air. *Applied Surface Science, 473,* 261–265.
12. Ramos, S. M. M., Pirat, C., & Cottin-Bizonne, C. (2019). Stability of frozen water droplets on highly hydrophobic porous surfaces: Temperature effects. *Applied Surface Science, 469,* 864–869.
13. Koch, K., & Barthlott, W. (2009). Superhydrophobic and superhydrophilic plant surfaces: An inspiration for biomimetic materials. *Philosophical Transactions of the Royal Society A, 367,* 1487–1509.
14. Liu, P., Niu, L., Tao, X., Li, X., Zhang, Z., & Yu, L. (2018). Preparation of superhydrophobic–oleophilic quartz sand filter and its application in oil–water separation. *Applied Surface Science, 447,* 656–663.
15. Zhang, M., Wang, C., Wang, S., Shi, Y., & Li, J. (2012). Fabrication of coral-like superhydrophobic coating on filter paper for water–oil separation. *Applied Surface Science, 261,* 764–769.
16. Jung, Y., Jung, K. K., Park, B. G., & Ko, J. S. (2018). Capacitive oil detector using hydrophobic and oleophilic PDMS sponge. *International Journal of Precision Engineering and Manufacturing-Green Technology, 5,* 303–309.
17. Kim, D., Kim, H., Kim, S. W., Kim, D. R., & Lee, K.-S. (2015). Experimental investigation of frost retardation for superhydrophobic surface using a luminance meter. *International Journal of Heat and Mass Transfer, 87,* 491–496.
18. Barthlott, W., & Neinhuis, C. (1997). Purity of the sacred lotus, or escape from contamination in biological surfaces. *Planta, 202,* 1–8.
19. Parkin, I. P., & Palgrave, R. G. (2005). Self-cleaning coatings. *Journal of Materials Chemistry, 15,* 1689.
20. Bhushan, B., Jung, Y. C., & Koch, K. (2009). Micro-, nano- and hierarchical structures for superhydrophobicity, self-cleaning and low adhesion. *Philosophical Transactions of the Royal Society A, 367,* 1631–1672.
21. Daniello, R. J., Waterhouse, N. E., & Rothstein, J. P. (2009). Drag reduction in turbulent flows over superhydrophobic surfaces. *Physics of Fluids, 21,* 085103.
22. Krishnan, K. G., Milionis, A., Loth, E., Farrell, T. E., Crouch, J. D., & Berry, D. H. (2017). Influence of hydrophobic and superhydrophobic surfaces on reducing aerodynamic insect residues. *Applied Surface Science, 392,* 723–731.
23. Tuo, Y., Chen, W., Zhang, H., Li, P., & Liu, X. (2018). One-step hydrothermal method to fabricate drag reduction superhydrophobic surface on aluminum foil. *Applied Surface Science, 446,* 230–235.
24. Ma, M., & Hill, R. M. (2006). Superhydrophobic surfaces. *Current Opinion in Colloid & Interface Science, 11,* 193–202.
25. Gong, D., Long, J., Jiang, D., Fan, P., Zhang, H., Li, L., et al. (2016). Robust and stable transparent superhydrophobic polydimethylsiloxane films by duplicating via a femtosecond laser-ablated template. *ACS Applied Materials & Interfaces, 8,* 17511–17518.
26. Davaasuren, G., Ngo, C.-V., Oh, H.-S., & Chun, D.-M. (2014). Geometric study of transparent superhydrophobic surfaces

of molded and grid patterned polydimethylsiloxane (PDMS). *Applied Surface Science, 314,* 530–536.
27. Xie, L., Tang, Z., Jiang, L., Breedveld, V., & Hess, D. W. (2015). Creation of superhydrophobic wood surfaces by plasma etching and thin-film deposition. *Surface and Coatings Technology, 281,* 125–132.
28. Ebert, D., & Bhushan, B. (2016). Transparent, superhydrophobic, and wear-resistant surfaces using deep reactive ion etching on PDMS substrates. *Journal of Colloid and Interface Science, 481,* 82–90.
29. Rezayi, T., & Entezari, M. H. (2016). Toward a durable superhydrophobic aluminum surface by etching and ZnO nanoparticle deposition. *Journal of Colloid and Interface Science, 463,* 37–45.
30. Zang, D., Liu, F., Zhang, M., Niu, X., Gao, Z., & Wang, C. (2015). Superhydrophobic coating on fiberglass cloth for selective removal of oil from water. *Chemical Engineering Journal, 262,* 210–216.
31. Zhang, Z., Ge, B., Men, X., & Li, Y. (2016). Mechanically durable, superhydrophobic coatings prepared by dual-layer method for anti-corrosion and self-cleaning. *Colloids and Surfaces A: Physicochemical and Engineering Aspects, 490,* 182–188.
32. Liu, S., Liu, X., Latthe, S. S., Gao, L., An, S., Yoon, S. S., et al. (2015). Self-cleaning transparent superhydrophobic coatings through simple sol–gel processing of fluoroalkylsilane. *Applied Surface Science, 351,* 897–903.
33. Wu, X., Fu, Q., Kumar, D., Ho, J. W. C., Kanhere, P., Zhou, H., et al. (2016). Mechanically robust superhydrophobic and superoleophobic coatings derived by sol–gel method. *Materials and Design, 89,* 1302–1309.
34. Moon, I. Y., Kim, B. H., Lee, H. W., Oh, Y.-S., Kim, J. H., & Kang, S.-H. (2019). Superhydrophobic polymer surface with hierarchical patterns fabricated in hot imprinting process. *International Journal of Precision Engineering and Manufacturing-Green Technology*. https://doi.org/10.1007/s40684-019-00094-5.
35. Sojoudi, H., Wang, M., Boscher, N. D., McKinley, G. H., & Gleason, K. K. (2016). Durable and scalable icephobic surfaces: Similarities and distinctions from superhydrophobic surfaces. *Soft Matter, 12,* 1938–1963.
36. Bhushan, B., & Multanen, V. (2019). Designing liquid repellent, icephobic and self-cleaning surfaces with high mechanical and chemical durability. *Philosophical Transactions of the Royal Society A, 377,* 20180270.
37. Wang, F., Liang, C., Yang, M., Fan, C., & Zhang, X. (2015). Effects of surface characteristic on frosting and defrosting behaviors of fin-tube heat exchangers. *Applied Thermal Engineering, 75,* 1126–1132.
38. Justo Alonso, M., Liu, P., Mathisen, H. M., Ge, G., & Simonson, C. (2015). Review of heat/energy recovery exchangers for use in ZEBs in cold climate countries. *Building and Environment, 84,* 228–237.
39. So, H., & Senesky, D. G. (2017). Effect of frost formation on operation of GaN ultraviolet photodetectors at low temperatures. *IEEE Sensors Journal, 17,* 4752–4756.
40. Nosonovsky, M., & Hejazi, V. (2012). Why superhydrophobic surfaces are not always icephobic. *ACS Nano, 6,* 8488–8491.
41. Hejazi, V., Sobolev, K., & Nosonovsky, M. (2013). From superhydrophobicity to icephobicity: Forces and interaction analysis. *Scientific Reports, 3,* 2194.
42. Kulinich, S. A., Farhadi, S., Nose, K., & Du, X. W. (2011). Superhydrophobic surfaces: Are they really ice-repellent? *Langmuir, 27,* 25–29.
43. Jung, S., Dorrestijn, M., Raps, D., Das, A., Megaridis, C. M., & Poulikakos, D. (2011). Are superhydrophobic surfaces best for icephobicity? *Langmuir, 27,* 3059–3066.
44. Ambrosi, A., & Pumera, M. (2016). 3D-printing technologies for electrochemical applications. *Chemical Society Reviews, 45,* 2740–2755.
45. Rengier, F., Mehndiratta, A., von Tengg-Kobligk, H., Zechmann, C. M., Unterhinninghofen, R., Kauczor, H.-U., et al. (2010). 3D printing based on imaging data: Review of medical applications. *International Journal of Computer Assisted Radiology and Surgery, 5,* 335–341.
46. Khare, V., Sonkaria, S., Lee, G.-Y., Ahn, S.-H., & Chu, W.-S. (2017). From 3D to 4D printing—design, material and fabrication for multi-functional multi-materials. *International Journal of Precision Engineering and Manufacturing-Green Technology, 4,* 291–299.
47. Lee, J., Kim, H.-C., Choi, J.-W., & Lee, I. H. (2017). A review on 3D printed smart devices for 4D printing. *International Journal of Precision Engineering and Manufacturing-Green Technology, 4,* 373–383.
48. Dudek, P. (2013). FDM 3D printing technology in manufacturing composite elements. *Archives of Metallurgy and Materials, 58,* 1415–1418.
49. Goyanes, A., Chang, H., Sedough, D., Hatton, G. B., Wang, J., Buanz, A., et al. (2015). Fabrication of controlled-release budesonide tablets via desktop (FDM) 3D printing. *International Journal of Pharmaceutics, 496,* 414–420.
50. Chai, X., Chai, H., Wang, X., Yang, J., Li, J., Zhao, Y., et al. (2017). Fused deposition modeling (FDM) 3D printed tablets for intragastric floating delivery of domperidone. *Scientific Reports, 7,* 2829.
51. Garcia, C. R., Rumpf, R. C., Tsang, H. H., & Barton, J. H. (2013). Effects of extreme surface roughness on 3D printed horn antenna. *Electronics Letters, 49,* 734–736.
52. Villegas, M., Cetinic, Z., Shakeri, A., & Didar, T. F. (2018). Fabricating smooth PDMS microfluidic channels from low-resolution 3D printed molds using an omniphobic lubricant-infused coating. *Analytica Chimica Acta, 1000,* 248–255.
53. Kang, B., Hyeon, J., & So, H. (2019). Facile microfabrication of 3-dimensional (3D) hydrophobic polymer surfaces using 3D printing technology. *Applied Surface Science*. https://doi.org/10.1016/j.apsusc.2019.143733.
54. Giordano, R. A., Wu, B. M., Borland, S. W., Cima, L. G., Sachs, E. M., & Cima, M. J. (1997). Mechanical properties of dense polylactic acid structures fabricated by three dimensional printing. *Journal of Biomaterials Science, Polymer Edition, 8,* 63–75.
55. Jeon, S., Han, J., Jeong, W., Son, J., Kim, J. B., & Kang, H.-W. (2019). Flexibility enhancement of poly(lactide-co-glycolide) for fused deposition modeling technology. *International Journal of Precision Engineering and Manufacturing-Green Technology*. https://doi.org/10.1007/s40684-019-00067-8.
56. Jiang, J., Stringer, J., Xu, X., & Zhong, R. Y. (2018). Investigation of printable threshold overhang angle in extrusion-based additive manufacturing for reducing support waste. *International Journal of Computer Integrated Manufacturing, 31,* 961–969.
57. Jiang, J., Xu, X., & Stringer, J. (2018). Support structures for additive manufacturing: A review. *Journal of Manufacturing and Materials Processing, 2,* 64.
58. Jiang, J., Lou, J., & Hu, G. (2019). Effect of support on printed properties in fused deposition modelling processes. *Virtual and Physical Prototyping, 14,* 308–315.
59. Zheng, Y., Gao, X., & Jiang, L. (2007). Directional adhesion of superhydrophobic butterfly wings. *Soft Matter, 3,* 178–182.
60. Chen, C.-M., & Yang, S. (2014). Directed water shedding on high-aspect-ratio shape memory polymer micropillar arrays. *Advanced Materials, 26,* 1283–1288.

Beomchan Kang received the B.S. degree from Seoul National University of Science and Technology, Korea, in 2015, and M.S. degree from Hanyang University, Korea, in 2018, where he is currently pursuing the Ph.D. degree in the Mechanical Engineering Department. His research interests are additive manufacturing, soft materials, and bio-inspired surfaces.

Jaebum Sung received the B.S. degree from Hanyang University, Korea, in 2019, where he is currently pursuing the M.S. and Ph.D. degrees in the Mechanical Engineering Department. His research interests include micro sensors for aeronautical applications, precision engineering, micromachining, microscale heat transfer, and thin film deposition.

Hongyun So received the B.S. degree from Hanyang University, Korea, in 2009, the M.S. degree from KAIST, Korea, in 2011, and the Ph.D. degree from the University of California, Berkeley, in 2014, all in mechanical engineering. He joined Stanford University in 2015 as a Post-Doctoral Scholar with the Aeronautics and Astronautics Department. He is currently an Assistant Professor with the Mechanical Engineering Department, Hanyang University. His research interests include design, modeling, and manufacturing of micro/nanosystems, harsh-environment sensors, and mechanical issues related to heat transfer and fluid mechanics.